



HAL
open science

Loose abrasive slurries for optical glass lapping

Jérôme Neauport, Julie Destribats, Cédric Maunier, Chrystel Ambard,
Philippe Cormont, B Pintault, Olivier Rondeau

► To cite this version:

Jérôme Neauport, Julie Destribats, Cédric Maunier, Chrystel Ambard, Philippe Cormont, et al.. Loose abrasive slurries for optical glass lapping. *Journal of Optics A: Pure and Applied Optics*, 2010, 49, pp.5736-5745. 10.1364/AO.49.005736 . cea-01217069

HAL Id: cea-01217069

<https://cea.hal.science/cea-01217069>

Submitted on 18 Oct 2015

HAL is a multi-disciplinary open access archive for the deposit and dissemination of scientific research documents, whether they are published or not. The documents may come from teaching and research institutions in France or abroad, or from public or private research centers.

L'archive ouverte pluridisciplinaire **HAL**, est destinée au dépôt et à la diffusion de documents scientifiques de niveau recherche, publiés ou non, émanant des établissements d'enseignement et de recherche français ou étrangers, des laboratoires publics ou privés.

Loose abrasive slurries for optical glass lapping

Jérôme Neauport,^{1,*} Julie Destribats,¹ Cédric Maunier,¹ Chrystel Ambard,²
Philippe Cormont,¹ B. Pintault,² and Olivier Rondeau²

¹Commissariat à l'Energie Atomique, Centre d'Etudes Scientifiques et Techniques d'Aquitaine (CEA CESTA),
F-33114, Le Barp, France

²Commissariat à l'Energie Atomique (CEA) Le Ripault, F-37260, Monts, France

*Corresponding author: jerome.neauport@projet-lmj.org

Received 11 May 2010; revised 26 August 2010; accepted 15 September 2010;
posted 17 September 2010 (Doc. ID 128314); published 12 October 2010

Loose abrasive lapping is widely used to prepare optical glass before its final polishing. We carried out a comparison of 20 different slurries from four different vendors. Slurry particle sizes and morphologies were measured. Fused silica samples were lapped with these different slurries on a single side polishing machine and characterized in terms of surface roughness and depth of subsurface damage (SSD). Effects of load, rotation speed, and slurry concentration during lapping on roughness, material removal rate, and SSD were investigated. © 2010 Optical Society of America

OCIS codes: 220.5450, 140.3330.

1. Introduction

Fusion class laser facilities such as Laser Mégajoule or the National Ignition Facility [1,2] use fused silica optics to transport and focus laser beams at the wavelength of 351 nm; in this context, the lifetime of fused silica optics when submitted to high laser fluences at this wavelength has been the subject of many studies. Various authors have shown that residual subsurface cracks existing in fused silica optics are likely to be precursors of laser damage [3–6]. Hence, efforts have been made by us and many others to measure and understand the impact of each manufacturing process step on the creation of subsurface damage (SSD) under the final fused silica surface [7–11]. In a previous contribution, we studied the impact of diamond grinding and proposed various characterization methods to evaluate the depth of SSD under ground and fine ground surfaces [12]. We herein focus on the next manufacturing step of the polishing process, which is the loose abrasive lapping.

Loose abrasive grinding or lapping is the operation where a mix of water and loose abrasive, called slur-

ry, is applied between a glass sample and a lapping plate. This operation occurs between milling or shaping, which can be done either with diamond grinding machines or large diameter loose abrasives, and the final polishing operation. The roles of loose abrasive grinding are to both remove SSD induced by the previous steps and to reduce the surface roughness. But loose abrasive lapping itself must also generate as little and as shallow SSD as possible since the material removal rate (MRR) of final polishing is rather low. If significant progress has been made in diamond grinding, with machines and technologies delivering always better and better surface roughness [13], loose abrasive lapping remains widespread in optical workshops. Moreover, its ease of use makes it very useful for many applications.

Buijs and Korpel-Van Houten studied loose abrasive lapping from a theoretical point of view [14]. Relating material removal to the formation of lateral fractures, the effects of lap and glass compositions on MRR were investigated. Following the studies of Izumitani [15], Lambropoulos *et al.* proposed an interpretation of the lapping hardness of a wide variety of optical materials, based on a material removal micromechanical model by lateral cracking [16]. More recently, Wang *et al.* studied the effect of lapping parameters with SiC abrasive slurries on surface

roughness and SSD depth [17]. All these contributions focus on lapping efficiency related to material parameters (workpiece, lapping plate) with less attention paid to slurry distribution and composition. In contrast, our goal in this report is to consider the role of the loose abrasive slurry in the lapping process of fused silica. Hence, 20 different slurries (Al_2O_3 , SiC, and B_4C) from four different manufacturers were tested using various lapping conditions. Manufactured samples as well as loose abrasive slurries were fully characterized. In the following sections, we briefly describe the sample preparation and the abrasive characterization. This is followed by a description of the sample characterization methods we used. In the final section, we discuss the results and propose our conclusions.

2. Experimental

A. Sample Preparation Methods

Round-shaped Corning 7980 fused silica samples, 50 mm diameter and 10 mm thick, were used for this study. Samples were first polished to ensure minimal residual SSD or at least with an extent that could be neglected compared to the SSD induced by a loose abrasive lapping step. Samples were then processed on a Logitech PM5 single side lapping and polishing machine [18]. Two types of cast iron lapping plates were used: grooved and not grooved. Varying processing conditions were tested with rotation speeds of some revolutions per minute to 70 rpm and loads of 0.8 to 2.8 kg (equivalent to 40 to 140 g/cm^2 for 50 mm diameter samples); the effect of slurry concentration was also considered. Continuous slurry feeding was ensured by the machine on the lap with a rate of approximately 1 drop per second while slurry was continuously agitated to avoid any kind of caking in the slurry tank.

Between each set of experiments using a given type of slurry, we thoroughly scrubbed, cleaned, and rinsed all the elements of the machine; each abrasive was also put in a dedicated tank. These cautions were adopted to avoid any kind of cross contamination of the slurries. We hence ensure that a given sample has only been in contact with the desired abrasive and not a mix of the previous abrasives used with the machine.

B. Type of Abrasives Tested and Their Characterization

Because they are used in most optical workshops today, we first focused our testing on aluminas. We investigated aluminas from four different suppliers, denoted respectively A, B, C, and D, with different particle sizes. Alternatively, we also lapped samples with some B_4C from supplier B and some SiC from both suppliers B and D.

To get a complete knowledge of the abrasive we used, each one was characterized by x-ray fluorescence to analyze its chemical composition and its impurities, by scanning electron microscope (SEM) to

examine grain shape, and by laser diffraction to determine the grain size distribution.

X-ray fluorescence analyses were carried out with a wavelength dispersive XRF S4 Pioneer (Bruker AXS, Karlsruhe, Germany) to check the chemical composition of abrasives and their impurities. The results confirm the purity of slurries. Minor quantities (about 100 mg kg^{-1}) of alkalines (Na, K), alkaline earth metals (Mg, Ca, Sr), light elements (Cl, S, C, P), metals and rare earth (Zn, Cu, Ga, V, Ti, Pr, Ce, La), and silicon were detected.

Each abrasive was gold-sputter coated and observed with a scanning electron microscope (SEM) (LEO 435 VP, LEO Electron Microscopy Ltd, Cambridge, UK) in order to examine grain shape. Then laser diffraction was used to determine grain size distribution. This method can be used for particle size analysis because the diffractive angle of one particle is correlated to its size. Commercial laser diffractometers determine the particle size distribution of a powder by assuming that the scattering of an ensemble of particles is, within certain limits, identical to the sum of the individual scattering patterns of all particles present. Two optical models can be used to best fit the measured scattering pattern and so go back to a sphere size distribution. The Fraunhofer model assumes that only diffraction occurs. Particles are opaque and nonporous and the optical properties of the tested material are not considered. Mie theory considers diffusion and absorption of the laser by the particles in addition to diffraction, so the knowledge of optical properties is required. The Fraunhofer approximation can be used when particles are large compared to the wavelength of the laser light, typically when particle diameter is larger than 5 μm . Laser diffraction measurements were performed in distilled water with a Cilas model 1064L/D instrument by the diffraction of a laser light whose wavelength is 830 nm. Since efficient dispersion is important in order to achieve optimum measurement, 1 g of powder was predispersed in 10 ml of water in a beaker under constant stirring and ultrasonic treatment for 5 min. This slurry was introduced dropwise into the 1064L/D liquid module until a good obscuration level was reached. The size distribution was measured for 60 s while the suspension was continuously pumped and passed over the laser beam. Each measurement was repeated three times to ensure repeatability. Cumulative percentile values at 10%, 50%, and 90% of the particles, respectively denoted D10, D50, and D90, were computed from each size distribution. As an example, 50% of the particles have a diameter smaller than the value D50, which thus represents the medium size. D10 and D90 were used to determine the distribution span defined by D50/(D90-D10).

Table 1 summarizes the particle diameter of each abrasive used as stated by the supplier and the results of the abrasive size measurement we performed.

Most suppliers ensure that they use a unique process that grades the particles in size and shape more

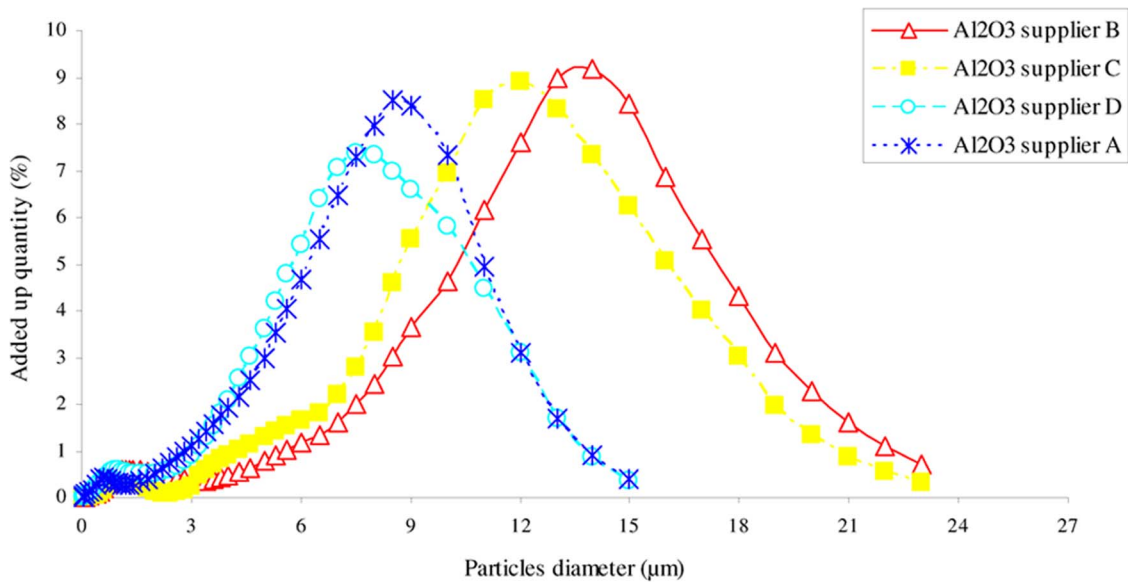


Fig. 1. (Color online) Size distribution of abrasive grains of different 9 μm aluminas.

closely than possible by using normal means. A comparison of the size distribution of four aluminas announced as 9 μm diameter by suppliers is shown in Fig. 1. The size distribution of the abrasive grains is Gaussian but the mean size is very different from one supplier to another, whereas the particle diameter (D50) is supposed to be the same. Another interesting point is to compare the shapes of abrasive grains. Figure 2(a) shows SEM pictures of Al_2O_3 particles. Although some of the aluminas produced by a special process should be characterized by platelet-shaped particles, photographs show that there are no significant differences among the shapes of alumina from all suppliers. We also compared the differences in

Table 1. Comparison of the Particle Diameter Announced by Supplier with Measures of the D50 and D90 of the Powder for Each Abrasive

Abrasive	Diameter Announced by Supplier (μm)	D50 (μm)	D90 (μm)
Al_2O_3 , supplier A	3	3	6
Al_2O_3 , supplier A	9	7	10
Al_2O_3 , supplier A	15	11	16
Al_2O_3 , supplier A	30	21	30
Al_2O_3 , supplier B	9	12	17
Al_2O_3 , supplier B	17	20	28
Al_2O_3 , supplier B	29	34	59
Al_2O_3 , supplier C	9	11	16
Al_2O_3 , supplier C	15	18	25
Al_2O_3 , supplier C	30	34	52
Al_2O_3 , supplier D	9	7	10
Al_2O_3 , supplier D	15	10	15
Al_2O_3 , supplier D	30	23	31
SiC, supplier B	9	12	17
SiC, supplier B	17	18	24
SiC, supplier B	29	36	57
SiC, supplier B	9	12	17
B_4C , supplier B	9	11	16
B_4C , supplier B	17	20	26
B_4C , supplier B	29	24	32

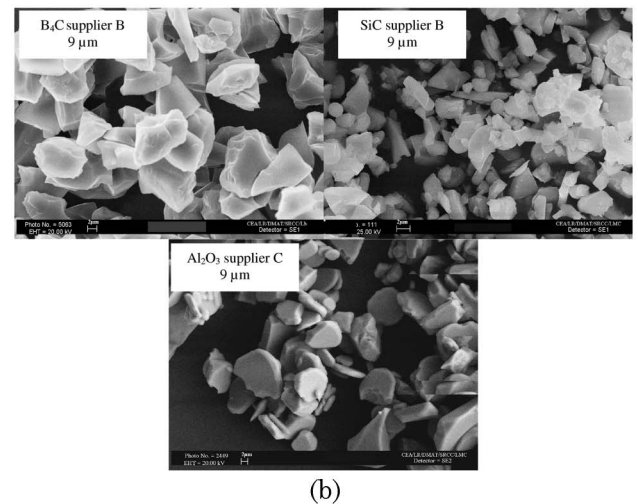
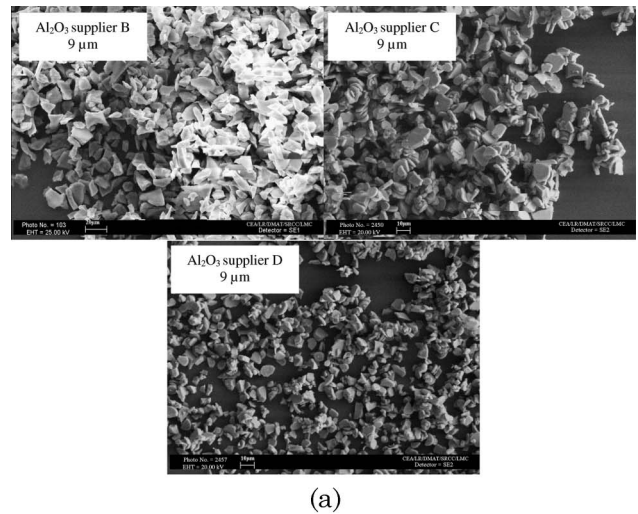


Fig. 2. (a) Typical SEM pictures of 9 μm Al_2O_3 particles. (b) SEM pictures of 9 μm Al_2O_3 , SiC, and B_4C particles.

shape of Al₂O₃, SiC, and B₄C particles for the same average particle size. Figure 2(b) compares the SEM images of particles for an average size of 9 μm. It can be seen that alumina particles exhibit smooth edges with platelet shapes as shown before, while B₄C and SiC particles, in particular, exhibit sharp edges with more random shapes.

C. Surface Roughness Measurements

A PHYNIX TR200 stylus profilometer was used to measure the average surface roughness (Ra) and peak-to-valley (Rt) surface roughness of each lapped sample. This profilometer is equipped with a 5 μm radius and 90° angle probe pin. Ra in a range of

0.01 to 40 μm and Rt in a range of 0.02 to 160 μm (maximum tip deflection) can be measured with this apparatus with a resolution of 0.001 μm. Sixteen measurements, equally placed radially with a scanning length of 4 mm, were done on the surface of each sample to compute Ra and Rt. For each sample, the Rt reported in Table 2 is the maximal value obtained among the whole set of 16 measurements equally distributed on the full sample surface.

D. SSD Measurements

Various methods have been proposed to measure SSD. We qualified and compared some of them on ground surfaces in a previous work [12]. Conse-

Table 2. Relationship between Maximal Surface Roughness Rt and SSD Depth as Measured by the Acid Etching Method

Sample	Experimental Conditions					Maximal Surface Roughness Rt	SSD Depth	<i>k</i>
	Abrasive	Grain Size	Speed	Load	Concentration			
S1	Al ₂ O ₃ , supplier C	9 μm	50 rpm	2.8 kg	13.3 vol. %	3.6	11.7	3.3
S2	Al ₂ O ₃ , supplier A	3 μm	5 rpm	2.8 kg	13.3 vol. %	2.1	7.5	3.6
S3	Al ₂ O ₃ A	3 μm	25 rpm	2.8 kg	13.3 vol. %	1.5	5.1	3.4
S4	Al ₂ O ₃ A	15 μm	50 rpm	2.8 kg	6.7 vol. %	3.3	11.9	3.6
S5	Al ₂ O ₃ A	15 μm	50 rpm	2.8 kg	20 vol. %	4.9	13.1	2.7
S6	Al ₂ O ₃ A	3 μm	50 rpm	1.8 kg	13.3 vol. %	1.6	4.7	2.9
S7	Al ₂ O ₃ A	3 μm	50 rpm	2.8 kg	6.7 vol. %	1.5	4.7	3.1
S8	Al ₂ O ₃ A	3 μm	50 rpm	0.8 kg	13.3 vol. %	1.6	5	3.1
S9	Al ₂ O ₃ A	3 μm	50 rpm	2.8 kg	20 vol. %	1.3	4.3	3.3
S10	Al ₂ O ₃ A	15 μm	5 rpm	2.8 kg	13.3 vol. %	5.1	16.6	3.3
S11	Al ₂ O ₃ A	15 μm	25 rpm	2.8 kg	13.3 vol. %	4.5	11.3	2.5
S12	Al ₂ O ₃ A	15 μm	70 rpm	2.8 kg	13.3 vol. %	3.4	13.8	4.1
S13	Al ₂ O ₃ A	15 μm	50 rpm	0.8 kg	13.3 vol. %	4.9	14.1	2.9
S14	Al ₂ O ₃ A	15 μm	50 rpm	2.8 kg	13.3 vol. %	3.9	12.1	3.1
S15	Al ₂ O ₃ A	15 μm	50 rpm	1.8 kg	13.3 vol. %	4.1	11.7	2.9
S16	Al ₂ O ₃ A	9 μm	50 rpm	2.8 kg	13.3 vol. %	2.8	11.2	4.0
S17	Al ₂ O ₃ A	3 μm	50 rpm	2.8 kg	13.3 vol. %	1.4	4.3	3.1
S18	Al ₂ O ₃ D	15 μm	5 rpm	2.8 kg	13.3 vol. %	4.3	12.1	2.8
S19	Al ₂ O ₃ D	15 μm	70 rpm	2.8 kg	13.3 vol. %	3.1	8.6	2.8
S20	Al ₂ O ₃ D	15 μm	25 rpm	2.8 kg	13.3 vol. %	3.6	11.3	3.1
S21	Al ₂ O ₃ D	15 μm	50 rpm	0.8 kg	13.3 vol. %	5.3	15.5	2.9
S22	Al ₂ O ₃ D	15 μm	50 rpm	2.8 kg	13.3 vol. %	3.4	10.7	3.1
S23	Al ₂ O ₃ D	15 μm	50 rpm	1.8 kg	13.3 vol. %	4.2	12.4	3.0
S24	Al ₂ O ₃ D	30 μm	60 rpm	2.4 kg	6.7 vol. %	6.4	21.7	3.4
S25	Al ₂ O ₃ C	30 μm	60 rpm	2.4 kg	6.7 vol. %	7.5	31.7	4.2
S26	Al ₂ O ₃ A	3 μm	60 rpm	2.4 kg	20 vol. %	1.6	6	3.8
S27	Al ₂ O ₃ A	15 μm	60 rpm	2.4 kg	20 vol. %	4.3	12.5	2.9
S28	Al ₂ O ₃ A	9 μm	60 rpm	2.4 kg	20 vol. %	3.1	10.8	3.5
S29	Al ₂ O ₃ A	30 μm	60 rpm	2.4 kg	6.7 vol. %	10.4	25.6	2.5
S30	SiC, supplier B	9 μm	60 rpm	2.4 kg	20 vol. %	4.5	13.1	2.9
S31	Al ₂ O ₃ B	9 μm	60 rpm	2.4 kg	20 vol. %	3.2	11.7	3.7
S32	B ₄ C, supplier B	17 μm	60 rpm	2.4 kg	20 vol. %	7.2	21.1	2.9
S33	SiC, supplier D	9 μm	60 rpm	2.4 kg	20 vol. %	4.1	11.6	2.8
S34	B ₄ C, supplier B	9 μm	60 rpm	2.4 kg	20 vol. %	3.4	10.7	3.1
S35	B ₄ C, supplier B	29 μm	60 rpm	2.4 kg	6.7 vol. %	8.3	29.9	3.6
S36	SiC, supplier B	17 μm	60 rpm	2.4 kg	20 vol. %	6.7	19.2	2.9
S37	Al ₂ O ₃ B	17 μm	60 rpm	2.4 kg	20 vol. %	4.7	20.4	4.3
S38	SiC, supplier B	29 μm	60 rpm	2.4 kg	6.7 vol. %	7.4	30.6	4.1
S39	Al ₂ O ₃ B	29 μm	60 rpm	2.4 kg	6.7 vol. %	6.4	31.5	4.9
S40	Al ₂ O ₃ D	9 μm	60 rpm	2.4 kg	20 vol. %	3.6	12.2	3.4
S41	Al ₂ O ₃ C	9 μm	60 rpm	2.4 kg	20 vol. %	4.6	13.6	3.0
S42	Al ₂ O ₃ D	15 μm	60 rpm	2.4 kg	20 vol. %	4.7	12.9	2.7
S43	Al ₂ O ₃ C	15 μm	60 rpm	2.4 kg	20 vol. %	4.4	18.1	4.1
							Mean <i>k</i>	3.3

^a*k* represents the proportional factor in the relation SSD = *k* Rt.

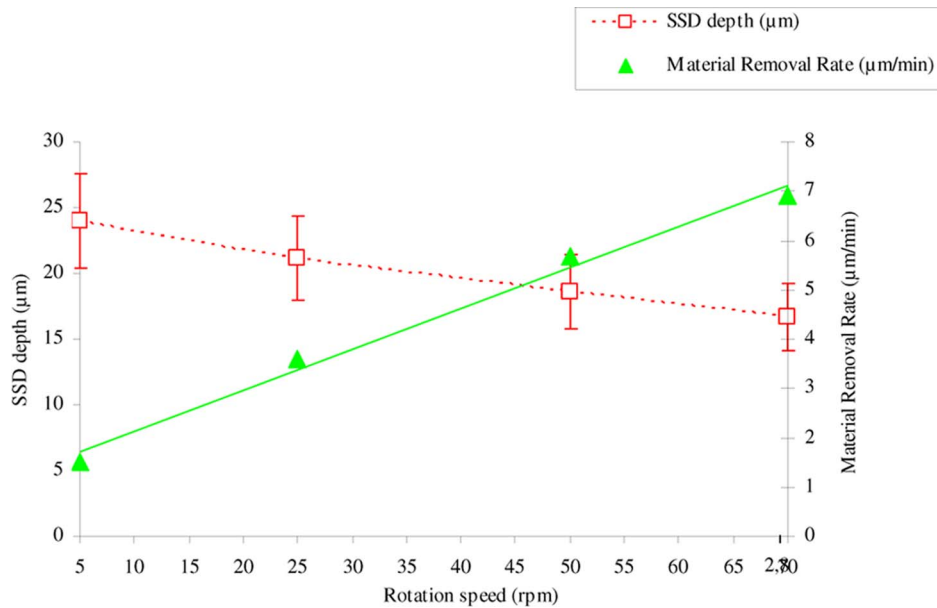


Fig. 3. (Color online) Influence of lapping rotation speed on the SSD depth and MRR (Al_2O_3 , $17 \mu\text{m}$, from supplier B, load = 2.4 kg , concentration = $13.3 \text{ vol. } \%$, lapping plate not grooved).

quently, because of its ease of implementation and its availability, we decided to measure SSD by means of acid etching. This principle has already been detailed elsewhere [12]. It consists in following the evolution of surface roughness R_t during hydrofluoric acid (HF) etching. Controlled thicknesses of silica are removed step by step by successive etchings. R_t is measured after each etching step using the procedure detailed in Subsection 2.C (16 measurements equally distributed on the whole sample surface). The position of roughness measurement spots can vary between two etchings. This means that we are not following the roughness evolution of a peculiar spot during etching, but rather the evolution of

the surface mean roughness. The roughness profile as a function of etched thickness can then be established. Since silica HF etching is isotropic, SSD of the silica sample is converted into roughness by the etching process. Hence, the maximal value of R_t among the whole set of measurements (i.e., 16 measurements times the number of etching steps performed) is equal to the SSD depth.

3. Results and Discussions

A. Relationship between Roughness and SSD Depth

Many authors have tried to establish a relation between SSD depth and surface roughness R_t or with

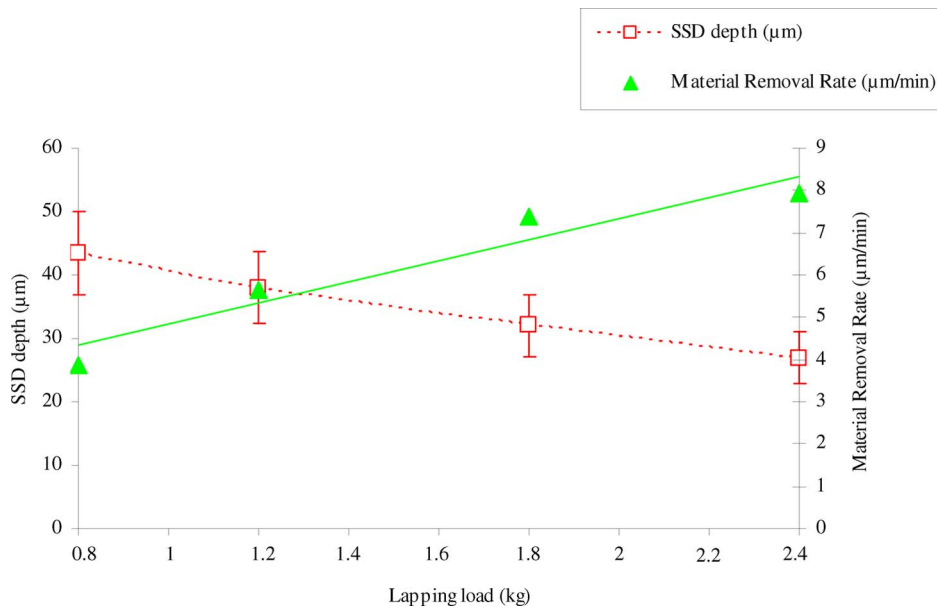


Fig. 4. (Color online) Influence of lapping load on the SSD depth and MRR (Al_2O_3 , $30 \mu\text{m}$, from supplier C, rotation speed = 50 rpm , concentration = $13.3 \text{ vol. } \%$, lapping plate not grooved).

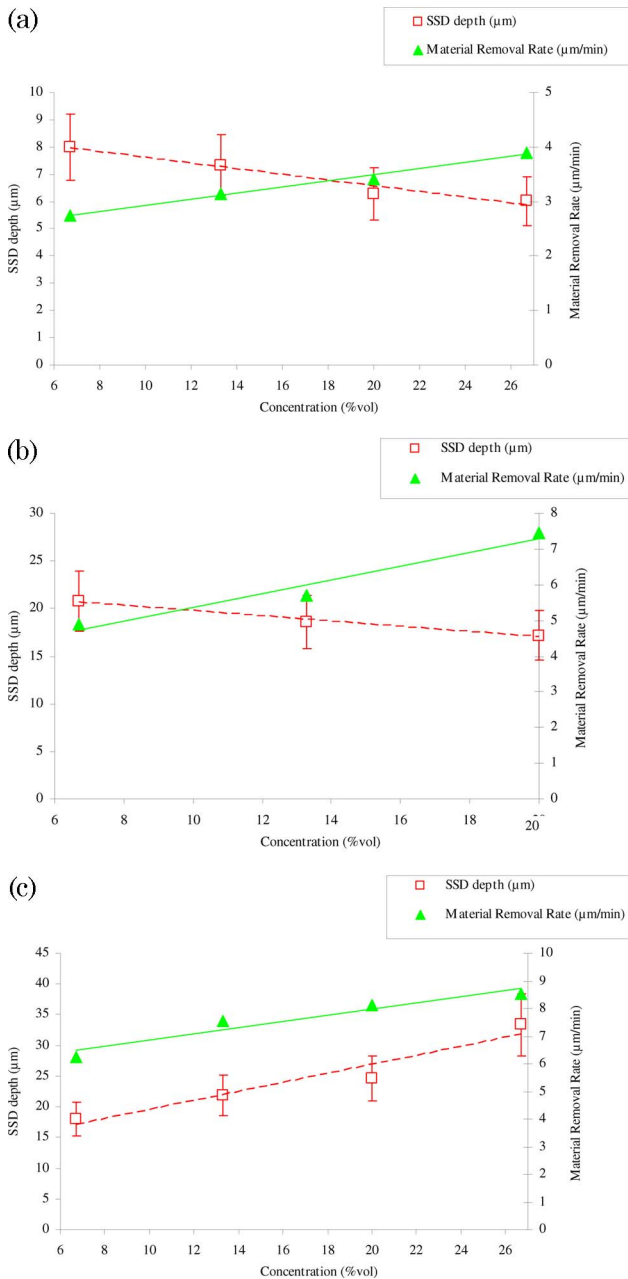


Fig. 5. (Color online) (a) Influence of slurry concentration on the SSD depth and MRR in the case of a powder with a low grain size (Al_2O_3 , $9 \mu\text{m}$, from supplier B, rotation speed = 50 rpm, load = 2.4 kg, lapping plate not grooved). (b) Influence of slurry concentration on the SSD depth and MRR in the case of a powder with an average grain size (Al_2O_3 , $17 \mu\text{m}$, from supplier B, rotation speed = 50 rpm, load = 2.4 kg, lapping plate not grooved). (c) Influence of slurry concentration on the SSD depth and MRR in the case of a powder with a high grain size (Al_2O_3 , $29 \mu\text{m}$, from supplier B, rotation speed = 50 rpm, load = 2.4 kg, lapping plate not grooved).

the mean size of the abrasive powder or grit used to generate the glass surface. Recent contributions mainly focus on a proportional relation between SSD depth and Rt, $\text{SSD depth} = k \text{ Rt}$, where k is a constant factor. We have shown in a previous work that part of the discrepancy of this proportional fac-

tor k , such as reported in the literature, was due to the various preparation methods and measuring principles retained for both surface roughness and SSD [12]. We evidenced a factor of $k = 9$ for a set of diamond ground samples, in good concordance with results from Miller *et al.* [19] and Suratwala *et al.* [11]. Our aim was also to evaluate the existence of such a relation for loose abrasive lapped samples using the same characterization methods. Table 2 presents the results of these experiments, detailing both manufacturing parameters (abrasive type, abrasive concentration, applied load, and rotation speed) and measurements of the manufactured samples. We notice that k is rather constant with a value of $k = 3.3 \pm 0.5$. This proportionality factor is herein only established with samples exhibiting SSD of more than $4.5 \mu\text{m}$ and Rt of more than 1.4 to $1.5 \mu\text{m}$. This value is in good agreement with results from Aleinikov, who reported a proportionality constant of $k = 3.93 \pm 0.17$ [7]. Suratwala *et al.* and Miller *et al.* more recently obtained a proportionality factor close to 9 [11,19]. Their measurements were made on both diamond ground silica samples and loose abrasive lapped samples. If we did confirm a proportionality factor close to 9 on diamond ground fused silica samples [12], current results show that this factor cannot be extended to loose abrasive lapped samples. It means that k is changing with the manufacturing process. We can outline that Hed and Edwards [9] noticed such a behavior with an increase of proportionality factor while going from loose abrasive lapped samples to bound abrasive lapped samples with a k of 6.4 ± 1.3 in the latter case. In what follows, a value of $k = 3.3 \pm 0.5$ is used to evaluate SSD from roughness measurements.

B. Effects of Lapping Parameters on SSD Depth

We investigated the role of lapping parameters on SSD depth and MRR. Lapping parameters studied are rotation speed, applied load, slurry concentration, lapping plate type (grooved or not grooved), and abrasive grain size. This study was conducted by lapping sets of samples with different types of abrasives, Al_2O_3 , B_4C , and SiC (see Table 1), using the sequence described in Subsection 2.A.

A typical example of the influence of the lapping rotation speed on MRR and SSD is presented in Fig. 3 with the following experimental conditions: Al_2O_3 $17 \mu\text{m}$ from supplier B, load = 2.4 kg, concentration = 13.3 vol. %, lapping plate not grooved. We can note that SSD depth decreases while MRR increases when the speed is increased from some revolutions per minute to the maximum value of 70 rpm.

The same kind of behavior is observed for the load as depicted on Fig. 4 (Al_2O_3 , $30 \mu\text{m}$ from supplier C, rotation speed = 50 rpm, concentration = 13.3 vol. %, lapping plate not grooved) with an increase of MRR according to Preston equation and a decrease of SSD when load is augmented.

Results obtained on the effect of load and rotation speed are given for Al_2O_3 slurries with some peculiar

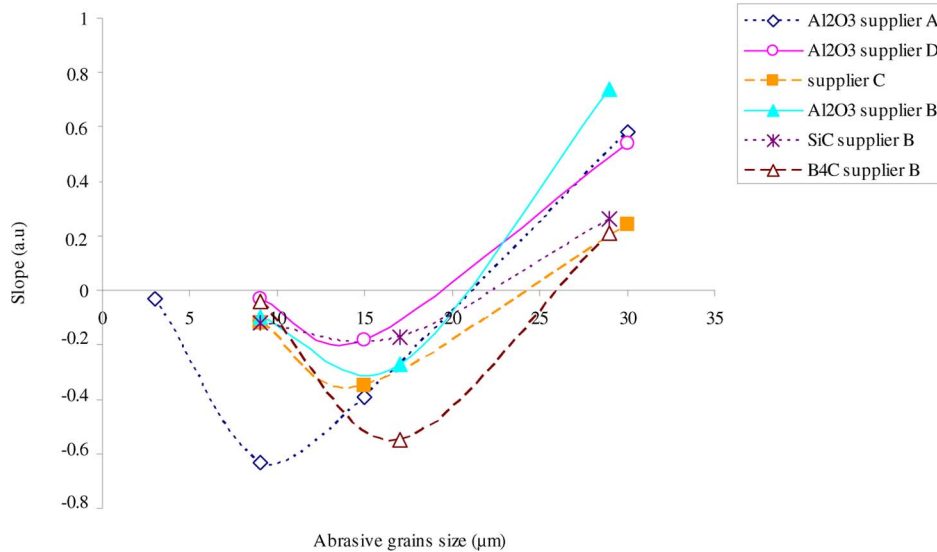


Fig. 6. (Color online) Slopes of SSD depth = f (concentration) for all the slurries.

abrasive diameters for illustration purposes, but similar tendencies were observed with all the abrasives we have tested. Some comments can then be made on the effect of load on SSD. Lambropoulos [20] and, later, Miller *et al.* [19] explained the material removal during grinding as multiple abrasive induced fractures. Evolution of roughness and SSD could then be calculated with an analogy to static blunt indentation. Doing so, these authors find that the proportionality ratio k is only a weak function of load P ($P^{1/6}$) and that SSD will grow with $P^{2/3}$. If our data confirm the weak dependence of the k ratio with load (see Table 2), they tend to contradict the later effect of load on SSD since SSD is decreasing with load in all our experiments.

The effect of slurry concentration on the SSD depth and MRR was also studied. Two different behaviors were noticed, depending on the size of the abrasive particles. Figures 5(a) and 5(b) depict, respectively, the cases of “small” (Al_2O_3 , 9 μm from supplier B)

and average (Al_2O_3 , 17 μm from supplier B) particles, while Fig. 5(c) illustrates the case of rather large particles (Al_2O_3 , 29 μm from supplier B). The experimental conditions were always as follows: rotation speed = 50 rpm, load = 2.4 kg, plate not grooved. In the case of a powder with a low or average grain size, it can be seen that, with an increase in the slurry concentration, the SSD depth decreases slightly, whereas MRR increases. Otherwise, in the case of a powder with a large grain size, the SSD depth and MRR both increase with an increase in the slurry concentration.

The slope of the linear evolution of SSD depth with concentration has been evaluated for all sets of experiments we carried out. This analysis is reported in Fig. 6. First, one can observe that the change of behavior occurs for all kinds of slurry for grains sizes between 20 and 25 μm . Then, Fig. 6 also indicates that, for each kind of abrasive, there is an optimal grain size for which SSD depth is strongly reduced by increasing the abrasive concentration in slurry.

Such behavior does not seem compatible with a static indent model as presented in [19], for example. Further measurements of the contact thickness during processing would be needed to address this point.

The effect of lapping plate configuration was studied as well. The SSD depth and MRR for two different kinds of plates are shown in Fig. 7 (Al_2O_3 , 30 μm from supplier A, rotation speed = 50 rpm, load = 2.4 kg, concentration = 13.3 vol. %). We can see that the SSD depth and MRR both increase with the use of a grooved plate.

Finally, the effect of the abrasive grains’ average diameter can be analyzed. SSD depth and MRR evolution for different abrasive sizes are given in Fig. 8 with the following experimental conditions: Al_2O_3 from supplier D, rotation speed = 50 rpm, load = 2.4 kg, concentration = 13.3 vol. %, plate not grooved. As suspected, MRR and SSD proportionately increase with an increase in the grain size.

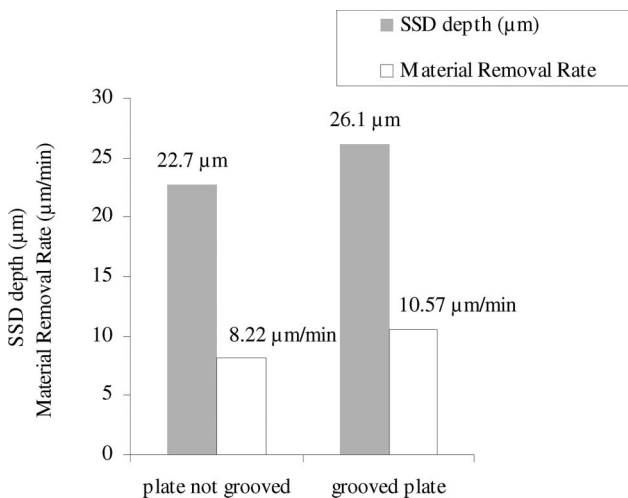


Fig. 7. Influence of the type of lapping plate on the SSD depth and MRR (Al_2O_3 , 30 μm , from supplier A, rotation speed = 50 rpm, load = 2.4 kg, concentration = 13.3 vol. %).

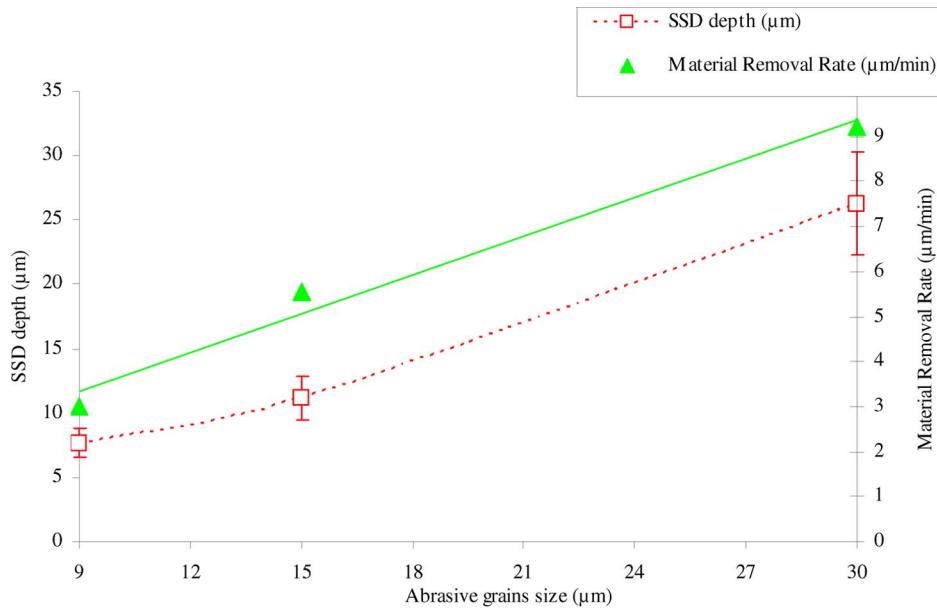


Fig. 8. (Color online) Influence of abrasive grain size on the SSD depth and MRR (Al_2O_3 , from supplier D, rotation speed = 50 rpm, load = 2.4 kg, concentration = 13.3 vol. %, plate not grooved).

We checked that this behavior fulfills the relation evidenced by Lambropoulos $0.3d^{0.68} < \text{SSD} < 2d^{0.85}$, where d is the mean abrasive size [21]. As presented in Fig. 9, our data are best fitted with a $0.74d^{1.04}$ power law.

The relative variation of the SSD depth and MRR according to the lapping parameters can then be summarized as presented in Table 3. We can see that a significant effect on SSD can be obtained by changing abrasive diameter, but also by making use of load and rotation speed.

C. Slurry Comparison

The results of the previous tests made it possible to compare the SSD depth created by the different powders, using the same experimental lapping parameters (rotation speed, load, slurry concentration, lapping plate) that were found to minimize SSD.

Comparison of all slurries is shown in Fig. 10 for this given set of experimental conditions: rotation speed = 60 rpm, load = 2.8 kg, concentration = 20 vol. % for low and average grain sizes, concentration = 13.3 vol. % for high grain size, plate not grooved. An attractive conclusion is that, for each abrasive grade, the depth of SSD created is always minimized by using aluminas.

With regard to suppliers, A or D seem to provide the best slurries for every abrasive grain size. We believe that this is mainly the result of good calibration of particle diameter, as can be seen in Fig. 1 and Table 1, where 9 μm aluminas from suppliers A and D exhibit the narrower size distributions and the lowest D90 values.

We also studied the evolution of MRR when changing the nature of the abrasive. Figure 11 presents the evolution of MRR for three different abrasives

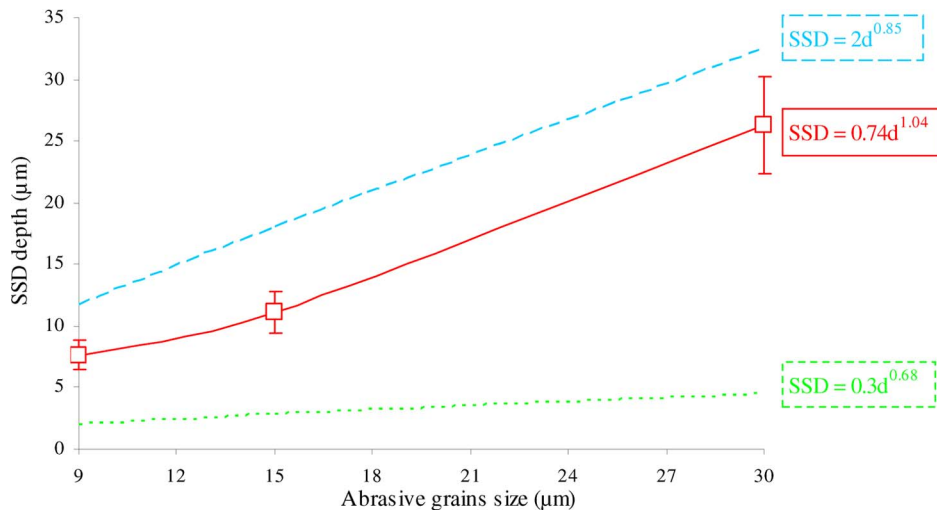


Fig. 9. (Color online) Evolution of SSD depth with mean particle size as stated by vendor. (Al_2O_3 , from supplier D, rotation speed = 50 rpm, load = 2.4 kg, concentration = 13.3 vol. %, plate not grooved). Comparison with law proposed by Lambropoulos [21].

Table 3. Relative Variation of SSD Depth and MRR according to Lapping Parameters

Lapping Parameters	Variation Range	Relative Variation of SSD Depth	Relative Variation of MRR
Lapping rotation speed	5–70 rpm	–30%	+550%
Lapping load	0.8–2.8 kg	–30%	+250%
Slurry concentration	6.7–26.7 vol. %	–25% (low grain size) +40% (high grain size)	+60%
Type of plate	grooved or not	+10%	+20%
Abrasive grain size	9–30 μm	+180%	+100%

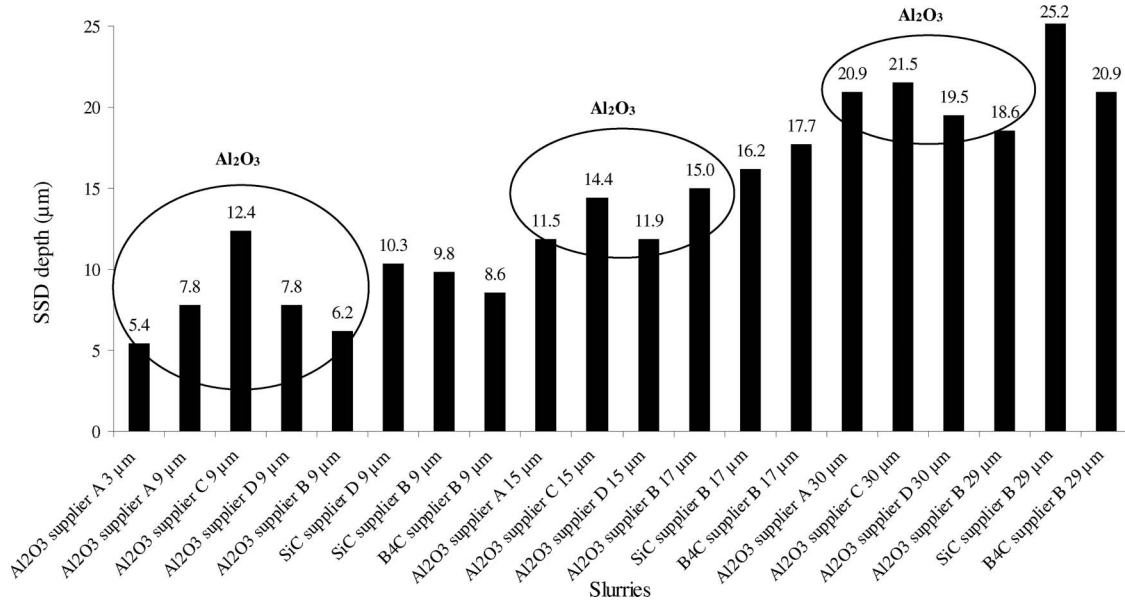


Fig. 10. Comparison of the SSD depth created by the different slurries with experimental conditions minimizing SSD (rotation speed = 60 rpm, load = 2.8 kg, concentration = 20 vol. % for low and mean grain size, concentration = 13.3 vol. % for high grain size, plate not grooved).

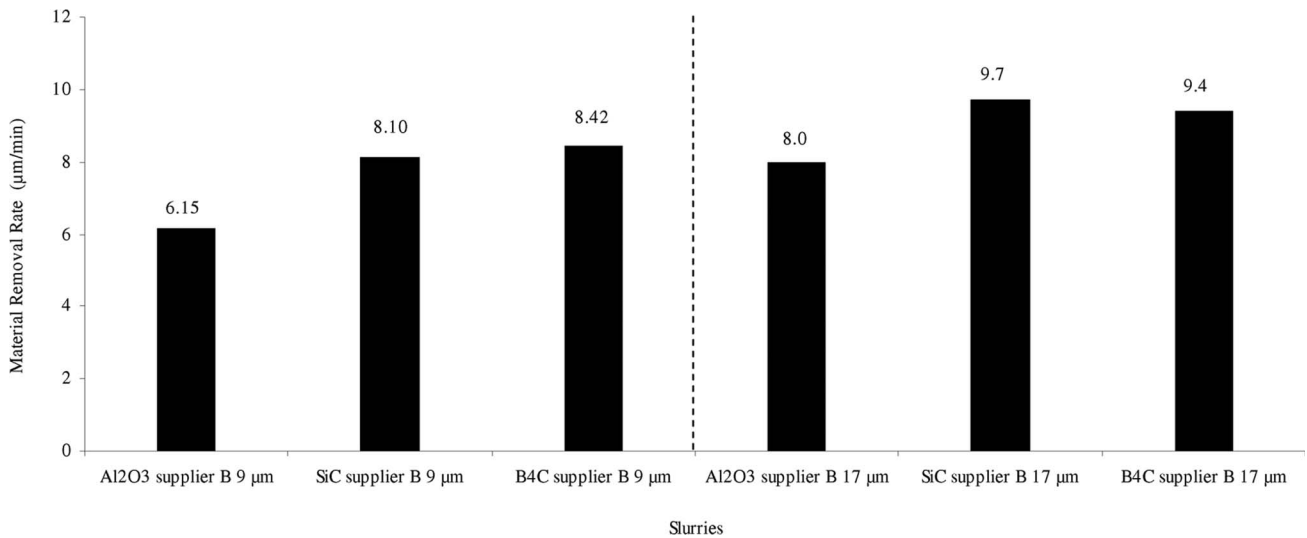


Fig. 11. Comparison of the MRR induced by the different slurries with experimental conditions minimizing SSD (rotation speed = 60 rpm, load = 2.8 kg, concentration = 20 vol. %).

from supplier B: alumina, SiC, and B₄C, of 9 and 17 μm at fixed lapping parameters (rotation speed = 60 rpm, load = 2.8 kg, concentration = 20 vol. %). For these three abrasives and two abrasive sizes, D50 and D90 values are very close to each

other (see Table 1). It can be seen from Fig. 11 that the MRR of SiC and B₄C is about 20% to 25% higher than that with alumina. Such behavior can be attributed to the rather sharp morphology of B₄C and SiC abrasives compared to alumina (see Subsection 2.B),

because, according to [19], the MRR due to sharp particles is likely to be higher than with blunt or smooth ones.

4. Conclusions

We investigated the effect of lapping conditions and abrasive types on both SSD and MRR in a loose abrasive lapping process. A wide range of abrasives in terms of suppliers and diameters was tested with different loads, rotation speeds, lapping plate configurations, and concentrations on a single side Logitech PM5 lapping and polishing machine. We evidenced that alumina exhibits inferior MRR but leads to lower SSD depth on fused silica as compared to other abrasives, such as B₄C or SiC. If, as already shown by others, decreasing particle size reduces SSD and MRR, then the effect of load and concentration is less obvious. The behavior shown (SSD decreasing while load increases, e.g.) tends to contradict the lapping models based on static indentation. Such models make the strong hypothesis of the existence of a single layer of particles between the lapping plate and the workpiece. We believe that, in some cases, multiple layers of particles could be involved. This hypothesis is currently being addressed both by *in situ* measurements and discrete element model simulations [22].

The authors acknowledge suppliers for kindly providing the various slurries for testing purposes. This work is supported by the Conseil Régional d'Aquitaine and is performed in the framework of the Etude et Formation en Surface Optique (EFESO) project.

References

1. M. L. André, "Status of the LMJ project," Proc. SPIE **3047**, 38–42 (1997).
2. W. H. Lowdermilk, "Status of the National Ignition Facility project," Proc. SPIE **3047**, 16–37 (1997).
3. N. Bloembergen, "Role of cracks, pores, and absorbing inclusions on laser damage threshold at surface of transparent dielectric," Appl. Opt. **12**, 661–664 (1973).
4. F. Y. Genin, A. Salleo, T. V. Pistor, and L. L. Chase, "Role of light intensification by cracks in optical breakdown on surfaces," J. Opt. Soc. Am. A **18**, 2607–2616 (2001).
5. M. D. Feit and A. M. Rubenchik, "Influence of subsurface cracks on laser induced surface damage," Proc. SPIE **5273**, 264–272 (2004).
6. H. Bercegol, P. Grua, D. Hébert, and J. P. Morreeuw, "Progress in the understanding of fracture related damage of fused silica," Proc. SPIE **6720**, 1–12 (2007).
7. F. K. Aleinikov, "The effect of certain physical and mechanical properties on the grinding of brittle materials," Sov. Phys. Tech. Phys. **2**, 2529–2538 (1957).
8. W. J. Rupp, "Mechanism of the diamond lapping process," Appl. Opt. **13**, 1264–1269 (1974).
9. P. Hed and D. F. Edwards, "Optical glass fabrication technology. 2. Relationship between surface roughness and subsurface damage," Appl. Opt. **26**, 4677–4680 (1987).
10. J. C. Randi, J. C. Lambropoulos, and S. D. Jacobs, "Subsurface damage in some single crystalline optical materials," Appl. Opt. **44**, 2241–2249 (2005).
11. T. Suratwala, L. Wong, P. Miller, M. D. Feit, J. Menapace, R. Steele, P. Davis, and D. Walmer, "Subsurface mechanical damage distributions during grinding of fused silica," J. Non-Cryst. Solids **352**, 5601–5617 (2006).
12. J. Neauport, C. Ambard, P. Cormont, N. Darbois, J. Destribats, C. Luitot, and O. Rondeau, "Subsurface damage measurement of ground fused silica parts by HF etching techniques," Opt. Express **17**, 20448–20456 (2009).
13. H. Policove and T. M. Moore, "Optics manufacturing technology moves towards automation," Laser Focus World **27**, 145–149 (1991).
14. M. Buijs and K. Korpel-Van Houten, "A model of lapping of glass," J. Mater. Sci. **28**, 3014–3020 (1993).
15. T. S. Izumitani, *Optical Glass* (American Institute of Physics, 1986), Chap. 4, p. 91J.
16. C. Lambropoulos, S. Xu, and T. Fang, "Loose abrasive lapping hardness of optical glasses and its interpretation," Appl. Opt. **36**, 1501–1516 (1997).
17. Z. Wang, Y. Wu, Y. Dai, and S. Li, "Subsurface damage distribution in the lapping process," Appl. Opt. **47**, 1417–1426 (2008).
18. Logitech Limited, Erskine Ferry Road, Old Kilpatrick, Glasgow, G60 5EU, Scotland, UK. <http://www.logitech.uk.com>
19. P. E. Miller, T. I. Suratwala, L. L. Wong, M. D. Feit, J. A. Menapace, P. J. Davis, and R. A. Steele, "The distribution of subsurface damage in fused silica," Proc. SPIE **5991**, 599101 (2005).
20. J. C. Lambropoulos, "Micromechanics of material-removal mechanisms from brittle surfaces," LLE Review **74**, 131–138 (1998).
21. J. C. Lambropoulos, "From abrasive size to subsurface damage in grinding," *Optical Fabrication and Testing*, OSA Technical Digest (Optical Society of America, 2000), pp. 17–18
22. I. Iordanoff, A. Battentier, J. Neauport, and J. L. Charles, "A discrete element model to investigate sub surface damage due to surface polishing," Tribol. Int. **41**, 957–964 (2008).